JOURNAL OF CATALYSIS 147, 123–132 (1994)

Morphology Study of MoS_2- and WS_2-Based Hydrotreating Catalysts by High-Resolution Electron Microscopy[1]

E. Payen,*,† R. Hubaut,* S. Kasztelan,‡ O. Poulet,*,[2] and J. Grimblot*

*Laboratoire de Catalyse Hétérogène et Homogène, U.R.A. CNRS 402, Université des Sciences et Technologies de Lille, Bâtiment C3, 59655 Villeneuve d'Ascq Cedex, France; †LASIR, U.P.R. CNRS 2641, Université des Sciences et Technologies de Lille, Bâtiment C5, 59655 Villeneuve d'Ascq Cedex, France; and ‡Institut Français du Pétrole, BP 311, 1-4 Avenue de Bois-Préau, 92500 Rueil-Malmaison, France

Received March 10, 1993; revised November 15, 1993

High-resolution electron microscopy (HREM) has been used to determine the morphology of MoS_2 (and WS_2) crystallites formed upon sulfidation of hydroprocessing catalysts which differ by (i) the loading of deposited molybdenum, (ii) the presence of Co or Ni promoters, (iii) the presence of additives such as P, F, Na, and Cs, and (iv) the nature of the support (γ-Al_2O_3, aluminates, zirconia). In general, the basis of comparison was established between samples having the same Mo (W) coverage in atom nm^{-2}. Based on the detection of more than 400 crystallites on several pictures of each sample, diagrams representing the length L of the elemental platelets as well as the number N of stacked layers have been obtained. Lengths higher than ~9.0 nm and stacking superior to five layers have never been observed. The mean $\bar{L}$ and $\bar{N}$ values are between 2.4–4.4 nm and 1.4–2.7 layers respectively. For selected samples, it appears that there exists a correlation between $\bar{N}$ and $\bar{L}$; $\bar{L}$ increases when $\bar{N}$ decreases, which reflects modifications in the stabilization energy of the disulfide crystallites or in the MoS_2-support interactions. On the other hand, we did not find evident correlation between the morphology changes and the variations of catalytic activity in toluene hydrogenation.

INTRODUCTION

MoS_2-γ-Al_2O_3 or WS_2-γ-Al_2O_3 catalysts promoted by cobalt or nickel are widely used for hydrotreating petroleum fractions to remove undesirable elements such as sulfur, nitrogen, oxygen, and/or trace amounts of nickel or vanadium present as porphyrin-like compounds. In recent catalyst formulations, other elements such as phosphorus have also been incorporated for improving the catalyst performances. Besides the conventional hydrodesulfurization (HDS) and hydrodenitrogenation (HDN) reactions, the Mo and W disulfide phases are also active in aromatic hydrogenation (1) or in CO methanation. In this latter case, oxide supports other than the classical transition aluminas are often preferred (2, 3).

Numerous complementary characterization techniques have been used for about two decades to describe the morphology of these supported systems (4–9). The architecture of the oxide precursor is primarily imposed by the nature of the support and by the preparation procedures. It is generally assumed that under a certain Mo (W) loading, well-dispersed molybdates or tungstates are present in a monolayer-like coverage. The Co or Ni ions may be in close interaction with these supported polyoxometallates, partly incorporated in the support or, at high loading, present as poorly dispersed oxides.

The reduction-sulfidation sequences, which are quite complex (10–13), transform the oxidic species initially present into pure (MoS_2, WS_2, Co_9S_8, NiS_x) or mixed Co(Ni)–Mo(W)–S sulfides. Nowadays, the presence of nanocrystals of MoS_2 or WS_2 in the sulfided catalyst is well established. However, it is still not clearly known how these phases are dispersed on the support. This is indeed a general problem in the field of supported catalysts. Besides indirect approaches such as chemisorption measurements or spectroscopic investigations, the use of high-resolution electron microscopy (HREM) is of decisive importance for answering this question (14, 15). Detection of MoS_2 and WS_2 particles in both unsupported and supported catalysts by HREM and observations of their respective oxidic precursors have already attracted considerable interest (7, 13–29). In these studies, layers of Mo disulfide are detected as threadlike structures whose lengths can be as small as about 2 nm. In the oxidic precursors, when well dispersed on the supports, the initial structures of molybdates or tungstates are not observed by HREM. Only in some cases (i.e., high Mo loaded catalysts), is there evidence for large crystallites of MoO_3 (27).

The beneficial property of alumina as a support is assumed to be due to its propensity to produce two-dimen-

[1] Paper presented at the 13th North American Meeting of the Catalysis Society, Pittsburgh, May 1993.

[2] Present address: Total Raffinage Distribution, BP 27, 76700 Harfleur, France.

0021-9517/94 $6.00

sional well-dispersed MoS_2 slabs (7). This result, however, is controversial, as other authors (22, 25) have also observed on Al_2O_3 stacking of layers in crystallites containing several parallel layers of MoS_2. Such stacked three-dimensional structures, where the fringe spacing corresponds to the Mo–Mo (W–W) distance in the *c* direction of MoS_2 (0.613 nm) or WS_2 (0.62 nm), may also be observed on unsupported catalysts (16–18, 29), or on alumina after high temperatures of sulfidation (7).

Sometimes results are statistically treated to give average data on both the number of stacked layers ($\overline{N}$) and on their length ($\overline{L}$) (20, 23, 25). Such analyses are useful to compare the role of supports on the MoS_2 (WS_2) dispersion. For example, Mauchausse *et al.* (23) when examining MoS_2 on various supports found $\overline{N}$ values increasing with the Mo loading. On alumina, the values are between 1 and 2. For similar Mo loading $\overline{N}$ increases in the sequence

$$\overline{N}\ (SiO_2) > \overline{N}\ (ZrO_2 > \overline{N}\ (Al_2O_3).$$

Conversely $\overline{L}$ is between 2 and 4 nm on alumina and the sequence is

$$\overline{L}\ (SiO_2) > \overline{L}\ (ZrO_2 > \overline{L}\ (Al_2O_3)$$

for samples of comparable Mo loading. Roles of other supports such as graphite (14), titania (24, 27), zirconia, and yttria (25) have also been discussed.

Another matter of debate is the orientation of the MoS_2 relative to the carrier-exposed surface. This point will be discussed below.

Most of the previous published work has been concerned with catalysts prepared by various methods using different supports and it stands to reason that the observed differences in morphology may be the result of the wide variety of preparation, activation and supports. This paper addresses the quantitative observation by HREM of sulfided catalysts whose oxidic precursors have already been well characterized (30–43). An attempt was made to identify differences in morphology of the MoS_2 (WS_2) crystallites due to changes in the catalyst composition or activation. Effects of parameters such as the presence of promoters (Co, Ni) or other additive elements (Na, Cs, F, P), the use of different oxide carriers (γ-alumina, Ni or Mg aluminate, zirconia), and the modification of the hydration degree of the MoO_3-γ-Al_2O_3 oxidic precursor before sulfidation will be considered. Tentative correlations with catalytic data (toluene hydrogenation) obtained on some sulfided catalysts will be discussed.

EXPERIMENTAL

Catalyst Preparation

Table 1 gives the nomenclature and the chemical composition of all the studied catalysts. The alumina-based catalysts use commercial γ-alumina carriers (from Rhône-Poulenc) which have an initial surface area of 238 $m^2\ g^{-1}$ (samples 1–6 and 15) or 252 $m^2\ g^{-1}$ (samples 10–14). The Ni or Mg aluminates and zirconia are laboratory-made supports (41, 42) with surface areas of, respectively, 142, 140, and 130 $m^2\ g^{-1}$. All the studied catalysts have been prepared by the pore filling method using solutions of ammonium heptamolybdate or paratungstate. For the catalysts promoted by Co or Ni (samples 5, 6, 9, and 12) and sample 10, which contains P, the initial impregnating solution also contained the desired amounts of Co^{2+} or Ni^{2+} as nitrates and P as phosphoric acid. After impregnation, the solids were dried at 380 K overnight and calcined in air at 773 K for 2 h. For sample 11, the alumina support was first modified by impregnation with a H_3PO_4 solution to deposit phosphorus in an amount corresponding to 6 wt.% of P_2O_5. After drying at 380 K for 24 h, the H_3PO_4-impregnated alumina was calcined in air at 773 K and then the procedure for depositing Mo was carried out. Na, Cs, and F were added to the calcined MoO_3-γ-Al_2O_3 sample by impregnation with a solution of Na or Cs nitrate or ammonium fluoride. The final calcination was performed at 773 K for 4 h. For comparison purposes, the Mo coverages were always chosen quite similar (2.3–2.9 Mo atoms nm^{-2}) whatever the support. All these catalysts have already been characterized, mainly in the oxidic state, by a variety of techniques such as X-ray photoelectron spectroscopy, ion scattering spectroscopy or laser Raman spectroscopy (30–43).

The sulfidation step, by a H_2S/H_2 (10% H_2S) mixture at 623 K for 3 h, was carried out on the powdered samples normally exposed to ambient air after the final calcination procedure. It was performed by raising the temperature at a rate of 5 K min^{-1} under the flow of the sulfiding gas mixture. For specific purposes, the oxidic precursor was dehydrated (treatment with dry O_2 at 700 K for 3 h) before sulfidation.

High-Resolution Electron Microscopy

The sulfided powder was ultrasonically dispersed in hexane for the preparation of the electron microscope grid covered with a thin carbon holed film. The instrument was a Jeol 100 CX microscope with a side entry tilt which provides instrument resolution over a continuous range of periodicities down to 0.3 nm. Interpretation of the HREM pictures of Mo or W sulfide-based catalysts is well documented (14, 15, 20). The black lines in the pictures, which strongly contrast with the support materials, correspond to the lattice images of MoS_2 or WS_2 fragments. These short black lines may be either single or in packets of up to about five parallel threads which correspond to the lamellar structure of the Mo (W) dichalcogenides. These lines come from nanocrystals viewed "edge on" (i.e., the layers lie roughly parallel to the electron beam). The

TABLE 1

Nomenclature and Chemical Composition of the Studied Catalysts

Catalyst number and nomenclature	Chemical composition			
	$MoO_3(WO_3)$ (wt.%)	Mo(W) coverage[a] atom nm^{-2}	CoO,NiO (wt.%)	Other additives (wt.%)[b]
1. $MoO_3(4)/Al_2O_3$	4.0	0.7		
2. $MoO_3(8)/Al_2O_3$	8.0	1.4		
3. $MoO_3(14)/Al_2O_3$	14.0	2.4		
4. $WO_3(21)/Al_2O_3$	20.9	2.3		
5. $CoO(3)\text{-}MoO_3(14)/Al_2O_3$	14.0	2.4	3	
6. $NiO(3)\text{-}MoO_3(14)/Al_2O_3$	14.0	2.4	2.9	
7. $MoO_3(8)/MgAl_2O_4$	8.5	2.5		
8. $MoO_3(8)/NiAl_2O_4$	8.5	2.4	[c]	
9. $NiO(2)\text{-}MoO_3(9)/ZrO_2$	9.3	2.9	2.1	
10. $P_2O_5(6)\text{-}MoO_3(14)/Al_2O_3$	14	2.3		6.0
11. $MoO_3(14)/P_2O_5(6)\text{-}Al_2O_3$	14	2.3		6.0
12. $NiO(3)\text{-}MoO_3(14)/P_2O_5(6)\text{-}Al_2O_3$	14	2.5		6.0
13. $CsMoO_3(14)/Al_2O_3$	14	2.5		5.0
14. $NaMoO_3(14)/Al_2O_3$	14	2.5		1.0
15. $FMoO_3(14)/Al_2O_3$	14	2.5		2.0

[a] The Mo or W coverages in atom nm^{-2} are calculated on the basis that the supported oxo-species are well dispersed on all the support areas, a situation which has been shown by XPS measurements on these oxidic precursors.

[b] On a P_2O_5 basis for P but only on an element basis for Na, Cs, and F.

[c] Ni of the support is not considered in the composition of the supported phase.

inclination was believed to be less than 5° (21). The observed spacing between the lines (0.61–0.62 nm) is consistent with the interplanar spacing characteristic of bulk MoS_2 (or WS_2). It was demonstrated (21) by computer simulation that a single layer of MoS_2 will give only a single black line at a defocus of 50–60 nm. Hence, with this proper defocussing, the black lines cannot be confused with Fresnel fringes. All these experimental details were taken into account for our own observations.

For each individual crystallite two parameters have been considered: these are the length L of the black lines, which roughly correspond to the lateral dimension (diagonal) of the observed MoS_2 (WS_2) platelets, and the number N of three-dimensional stacked layers. The following results are based on the observations of about 400–600 crystallites detected on several HREM pictures taken from different parts of the same sample dispersed on the microscope grid. From the tabulated results, it is possible to determine mean values according to

$$\bar{L} = \Sigma n_i \cdot L_i / \Sigma n_i$$

$$\bar{N} = \Sigma n_i \cdot N_i / \Sigma n_i,$$

where n_i is the number of elemental particles having the L_i, N_i characteristics. We assume here that in each crystallite with several layers, each of them has the same dimension which is roughly correct.

Catalytic Tests

In this paper, effects of the MoS_2 (WS_2) morphology (i.e., changes in $\bar{L}$, $\bar{N}$) have been tentatively analyzed in the light of the variation of hydrogenation activity measured on some catalysts by using toluene as model molecule. Two kinds of toluene hydrogenation tests were performed. In test I, toluene hydrogenation was performed on the sulfided catalysts at a total pressure of 6 MPa. Temperature was 623 K and the liquid hourly space velocity LHSV was 2 h^{-1}. The liquid feed composition was 20% toluene, 78% cyclohexane, and 2% thiophene. This last molecule ensures that the catalyst will not be desulfurized during the test. Test II was performed also with toluene as a probe molecule in a high-pressure catalytic flow reactor with a sulfur-free feed. Tests were carried out at 6 MPa, 623 K with a LHSV of toluene equal to 1.8 h^{-1}. Products were analyzed by gas chromatography with a flame ionization detector and Carbowax-glass columns. Experimental details of test II can be found in Refs. 39 and 40.

RESULTS

Typical HREM micrographs of some samples showing the presence of MoS_2 are presented in Fig. 1. These figures are really similar to those already reported (14, 15) exhibiting short black lines corresponding to the MoS_2 (WS_2)

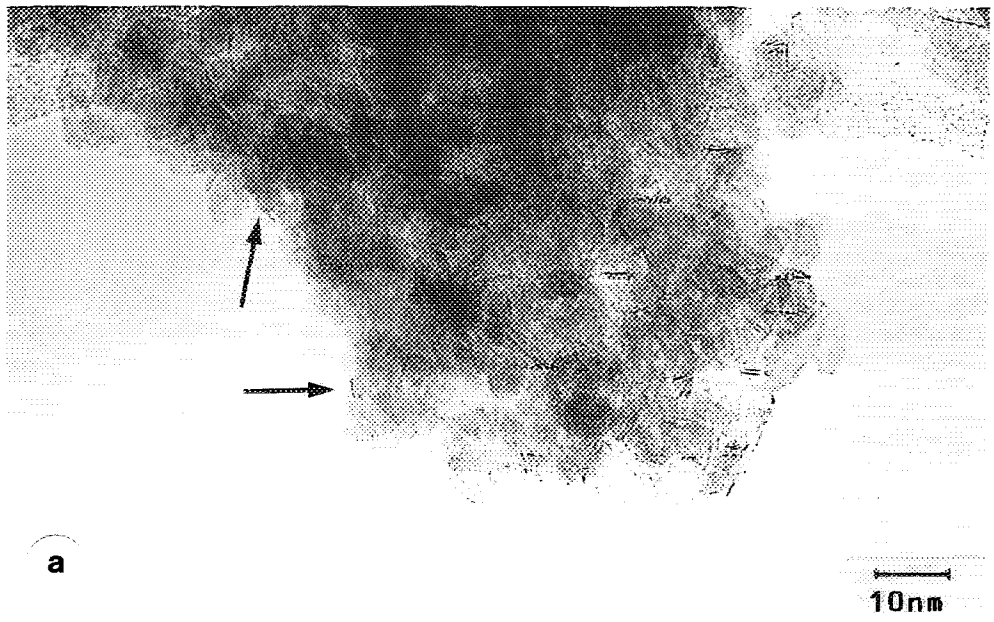

FIG. 1. HREM pictures of samples 6 (a), 10 (b), and 14 (c).

lamellar structure. It appears that the MoS_2 slabs are well dispersed on the support. Contrarily to the results on bulk Ni–Mo disulfides (16–18) no amorphous grains covered by fragments of MoS_2 layers are detectable in any case. Here, we only observe that single layers are dominant on the Mo-sulfided catalysts. On some other specimens whose micrographs are not reported here, multilayers containing crystallites are dominant.

Effect of the Mo Loading and of the Nature of the Supported Oxometallate Species (Samples 1 to 4)

In Fig. 2 the distributions (%) of the dimensions L and of the number N of stacked layers in the observed crystallites are reported. Sample 1 with a very low Mo loading (0.4 Mo atom nm^{-2}) is not represented in the diagrams because only very few MoS_2 layers were detected. Indeed, such a sample is generally described in the oxidic form as being constituted of isolated tetrahedral entities which are difficult to sulfide (30). Here, with the procedure of sulfidation used, these highly dispersed entities provide evidence of only a small number of MoS_2 crystallites. A statistical study of their morphology is therefore considered to be not representative. In samples 2 to 4, the single layer crystallites are dominant with representative length around 3.0 nm. Very few crystallites have dimensions over 8.0 nm and stacking over four layers. L and N evolutions are not quite identical among the three samples. The length distribution is broader for the WS_2–Al_2O_3 (sample 4), a result which could be related to the difficulty of sulfiding supported polytungstate species well enough by comparison with supported polymolybdate (36).

Effect of the Presence of Promoter (Samples 5, 6, and 8)

In sample 8, the nickel species are initially in the support as $NiAl_2O_4$, but it has been shown (43) that a fraction of it is migrating upon sulfidation to interact with the MoS_2 phase. The L, N distributions are reported in Fig. 3: similar features are obtained whatever the nature of the promoter and the way it is introduced. By comparison with sample 3 (14% MoO_3 on alumina, Fig. 2), the presence of Co or Ni induces stacking and a small increase in the length of the observed MoS_2 slabs. Indeed $\overline{N}$ = 1.4 and $\overline{L}$ = 3.5 nm for sample 3, whereas $\overline{N}$ = 1.5 and $\overline{L}$ = 4.0 nm for the Ni-promoted sample (no. 6) and $\overline{N}$ = 1.7 and $\overline{L}$ = 3.8 nm for the Co-promoted sample (no. 5) (see the value on the mean length and mean number of stacked layers in Table 2).

Effect of the Carrier (Samples 3, 6, 7, and 9)

Support effect on the activity and selectivity of hydrotreating catalysts has already been reviewed (44, 45). In Fig. 4 the L and N distributions for sample 7 supported on $MgAl_2O_4$ and sample 9 supported on zirconia are reported. It appears that the $\overline{N}$ values of sample 7 ($\overline{N}$ = 2.3) shifted towards more stacked crystallites by reference to catalyst with γ-Al_2O_3 as a support ($\overline{N}$ = 1.4). In both cases, the mean length is almost the same (3.5 vs 3.7 nm). For the promoted Ni–MoS_2 sample supported on zirconia, stacking is much more evident ($\overline{N}$ = 2.7, a value to compare with 1.5 relative to the classical Ni–MoS_2 supported on alumina, sample

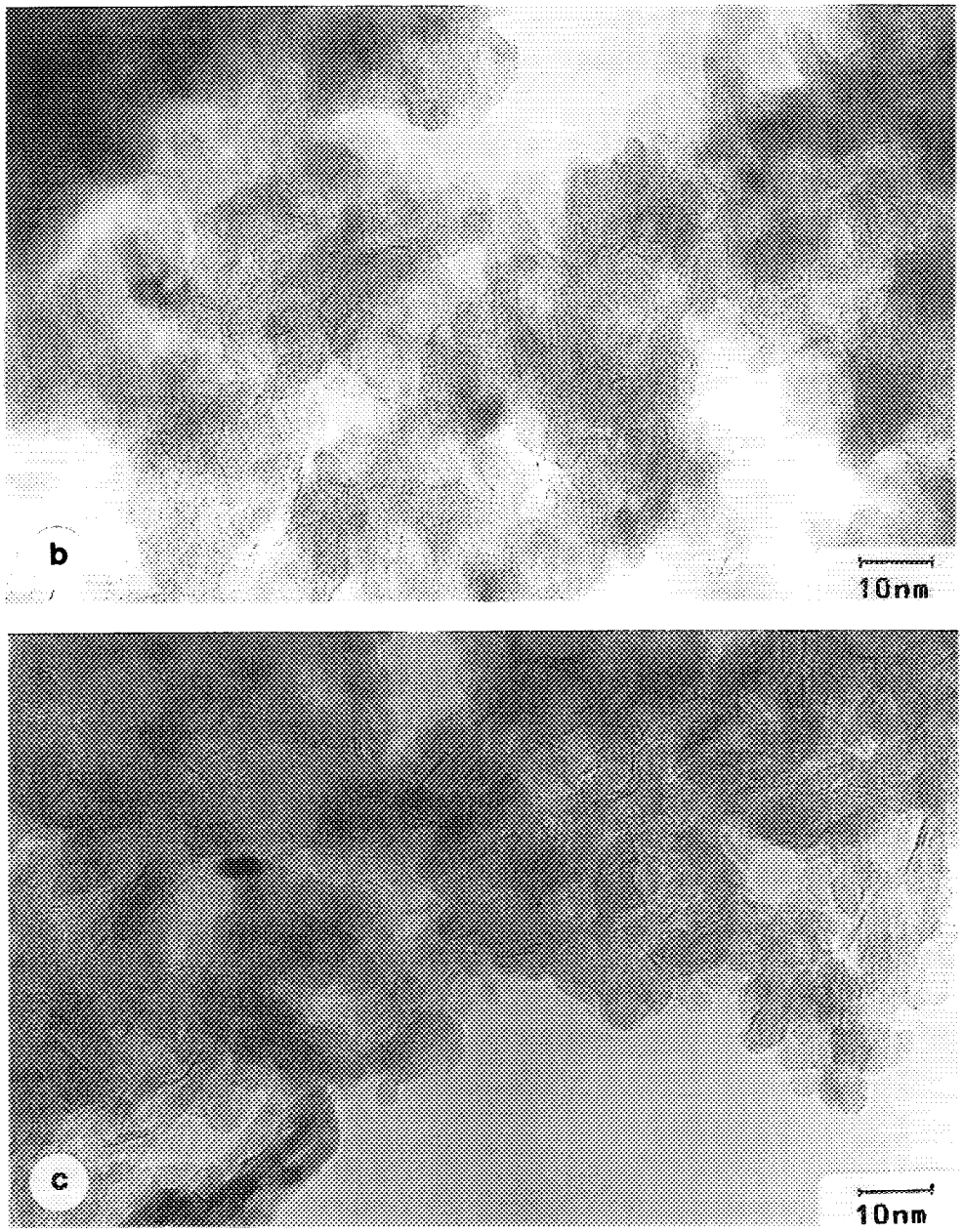

FIG. 1—Continued

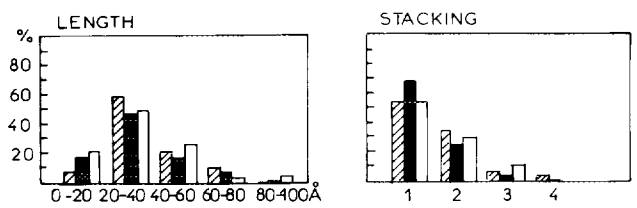

FIG. 2. Length (L) and layer stacking (N) distribution of MoS_2 or WS_2 crystallites on samples 2 (▨), 3 (■), and 4 (□).

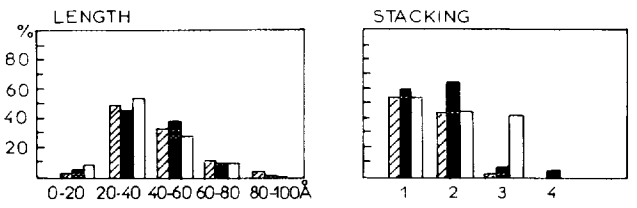

FIG. 3. Length (L) and layer stacking (N) distribution of MoS_2 crystallites in samples 6 (▨), 5 (■), and 8 (□).

TABLE 2

Mean Length ($\bar{L}$) and Number of Stacked Layers ($\bar{N}$) of Various Catalysts

Catalyst number	$\bar{N}$	$\bar{L}$(Å)
1. Mo(4)/Al		
2. Mo(8)/Al	1.6	32
3. Mo(14)/Al	1.4	35
4. W(21)/Al	1.6	24
4'. 4 dehydrated prior sulfidation	1.6	42
5. CoMo/Al	1.7	38
6. NiMo/Al	1.5	40
6'. 6 dehydrated prior sulfidation	2.0	30
7. Mo/MgAl	2.3	37
8. Mo/NiAl	1.6	39
9. NiMo/Zr	2.7	28
10. PMo/Al	2.5	32
11. Mo/PAl	1.6	44
12. NiMoP/Al	2.3	27
13. CsMo/Al	2.4	34
14. NaMo/Al	1.8	38
15. FMo/Al	2.7	33

6), whereas the mean length is really smaller (2.8 vs 4.0 nm).

Effect of Additives (Samples 10 to 15)

Figure 5 shows the influence of Na, Cs, or F on L and N distribution, whereas Fig. 6 illustrates the crystallite size distribution when P is present in the catalyst formulation.

In terms of mean values, it clearly appears that the Na, Cs, and F additives have a pronounced effect mainly on $\bar{N}$; the sequence is (Table 2)

$$\bar{N}_{Mo} \leq \bar{N}_{NaMo} < \bar{N}_{CsMo} < \bar{N}_{FMo}.$$

The effect on L is far less important as the $\bar{L}$ values vary between 3.3 and 3.8 nm. Nevertheless, it is interesting to note that the $\bar{L}$ evolution is opposite to the $\bar{N}$ evolution: stacking of the MoS_2 layers appears slightly detrimental to the dimension of the slabs. On the other hand, the presence of phosphorus induces an increase of the stacking which is very important for the sample prepared by the simultaneous impregnation method (sample 10). Conversely, the mean length of the slabs ($\bar{L}$ = 3.2 nm) of sample 10 is smaller than that of sample 3, whereas an increase of $\bar{L}$ occurs for sample 11 ($\bar{L}$ = 4.4 nm).

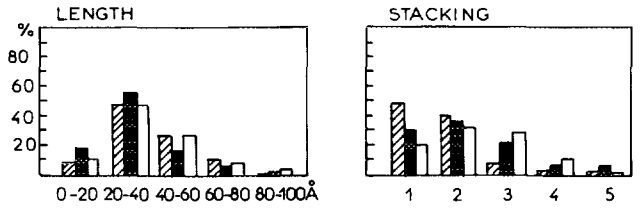

FIG. 5. Length (L) and layer stacking (N) distribution of MoS_2 crystallites in samples 14 (▨), 13 (■), and 15 (□).

The XPS results obtained on such catalysts clearly indicate that after the same sulfidation procedure the Mo 3*d* doublet is less resolved in the case of catalyst 10, whereas the spectra of samples 11 and 3 are quite similar (46). It can be estimated that the amount of the Mo^{VI} remaining species corresponds to 22%, whereas it corresponds to 15% in the case of samples 3 and 11. P may therefore influence the MoS_2 morphology and the extent of sulfidation of the supported oxomolybdate species. In sample 12, where Ni and Mo are deposited on a support containing already 6% of P_2O_5, the $\bar{N}$ and $\bar{L}$ values are respectively 2.3 and 2.7 nm; the presence of phosphorus induces stacking.

Effect of Sulfiding a Dehydrated Catalyst

Samples 4 (WO_3/Al_2O_3) and 6 ($Ni–MoO_3/Al_2O_3$) have been dehydrated before sulfidation by a calcination procedure in dry oxygen at 700 K. Previous results (11–13) have already shown that the mechanism of sulfidation and rates of the steps may be influenced by the hydrated/dehydrated state of the oxidic precursor but the final sulfided phase is always MoS_2 or WS_2. Here we found (Fig. 7 and Table 2) that the effect is quite opposite for samples 4 (WS_2) and 6 ($Ni–MoS_2$). For sample 4, $\bar{N}$ does not change but $\bar{L}$ increases from 2.4 to 4.2 nm upon dehydra-

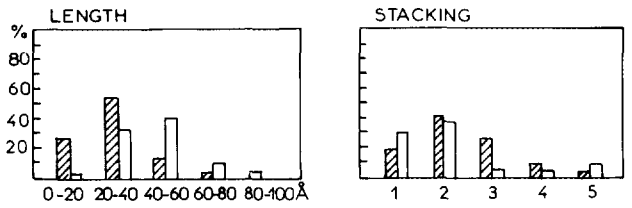

FIG. 4. Length (L) and layer stacking (N) distribution of MoS_2 crystallites in samples 9 (▨) and 7 (□).

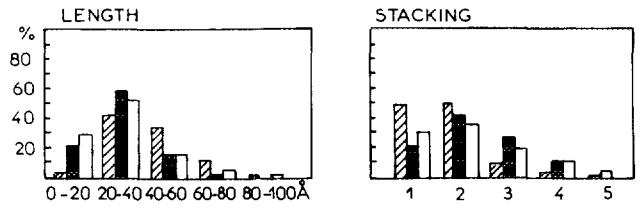

FIG. 6. Length (L) and layer stacking (N) distribution of MoS_2 crystallites in samples 11 (▨), 10 (■), and 12 (□).

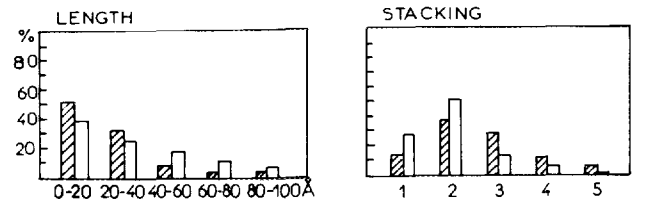

FIG. 7. Length (L) and layer stacking (N) distribution of MoS_2 or WS_2 crystallites of samples 4 (▨) and 6 (□) dehydrated in the oxidic form before sulfidation.

tion. For sample 6, $\bar{N}$ increases (1.5 to 2.0), whereas $\bar{L}$ decreases from 4.0 to 3.0 nm.

DISCUSSION

The results presented in this work concern the modifications, if any, of the morphology of the active MoS_2 (WS_2) active phases present in certain hydroprocessing catalysts in which different properties have been changed on purpose. However, the discussion should be conducted in the light of the debatable aspects relative to the use of HREM for elucidating details in the atomic distance range. Among the matters of debate of interest here, we can mention (i) the orientation of the Mo(W)S_2 layer(s) respective to the exposed planes of the support, (ii) the significance of the N and L values and of their changes (i.e., whether some catalysts contain very small sulfided particles which were not detected), (iii) identification of the key parameters which may induce significant morphology changes, and (iv) recognition of the consequences of the morphology evolution on the catalytic properties.

(i) *MoS_2 (WS_2) Layer Orientation*

The question of the orientation of the MoS_2 layers(s) relative to the exposed planes of the support has been examined several times (19–21, 27). In particular, Hayden and Dumesic (21) observed MoS_2 supported on thin films of alumina representing a nonporous support. In such a study, the alumina surface can have a rather well-known orientation (roughness effects and grain misorientation are negligible) with respect to the electron beam, which is an ideal situation. It was shown that the orientation of MoS_2 is highly dependent on the conditions of sulfidation; upon extensive sulfidation, the MoS_2 basal planes initially oriented perpendicular to the alumina plane become oriented parallel. On the other hand, large MoS_2 fringes well covering amorphous nodules have already been observed on nonporous carriers (27) or with the classical support (i.e., γ-Al_2O_3) for Mo loading in large excess of the monolayer capacity. In this case, the nodules are associated with the presence in the oxidic precursor of bulk MoO_3, which is easily detected by laser Raman spectroscopy. The determination of the MoS_2 orientation is still a real problem when the slabs represented by the dark lines on the micrographs (Fig. 1) are well dispersed on highly porous supports where all the support crystallites have (in principle) random orientation with respect to the electron beam. From the micrographs representing planar projections of three-dimensional samples with large heterogeneity, the opposite conclusion (20, 21) has been put forward, namely that the MoS_2 basal planes are roughly parallel or, conversely, perpendicular to the surface of the support crystals. In the present work, tentative information can be proposed only if in some zones in the micrographs, isolated support platelets are present with the possibility to observe the interface carrier/disulfide. In Fig. 1, the arrows indicate the presence of isolated alumina particles at the edge of which the MoS_2 platelet seems to lie flat. In the selected area of these samples, there is no sure evidence of MoS_2 standing up.

(ii) *Significance of the L and N Values*

For all the samples examined in this work, the number of crystallites detected and identified as MoS_2 layers (single or stacked) was always over 400; this allows one to establish statistics. However, the limits in the data reported here come mainly from the difficulty to obtain very small MoS_2 particles (i.e., particles which would have dimensions less than 1 nm) and to identify a single particle even if the orientation of the MoS_2 layer more or less accommodates to the morphology of the support. The MoS_2 sheets presumably form complicated networks but only portions having the c axis perpendicular to the incident beam direction are imaged. This could modify the observed length. This aspect was pointed out by Srinivasan *et al.* (27), who mentioned that the surface texture of the support affects the morphology of the MoS_2 crystallites, which could affect the detectability of some particles. These difficulties are probably of minor importance when comparing particle distribution on supports having similar surface area, texture, and structure (alumina, aluminate) but could be the reason for some artefacts with less conventional supports (e.g., zirconia). Nevertheless, the data reported here have to be considered as representative of what the experimentalists have seen on the micrograph pictures. The standard deviation in the statistical results varies between 1.5 and 2.0 nm. The representation of the data as histograms appears very informative and naturally incorporates the limits of the statistical analysis.

(iii) *Evolution of L and N*

The morphology of the MoS_2 (and WS_2) particles (Figs. 2–7), represented by their dimensional L and number of stacked layers N along the **c** axis perpendicular to the MoS_2 basal plane, has been found to be dependent on

various parameters such as the Mo loading (up to 2.4 Mo atom nm^{-2}), the nature of the support (γ-alumina, aluminate, or zirconia), and the presence in the catalyst formulation of classical promoters (Co, Ni) and other additives (P, Na, Cs, F). However, the main features of these results are the rather small changes in the morphology of the supported sulfide phase within the set of catalysts studied. In terms of mean $\overline{L}$ and $\overline{N}$ data, the limit values found are respectively (Table 2)

$$2.4 \text{ nm} < \overline{L} < 4.4 \text{ nm}$$

$$1.4 < \overline{N} < 2.7 \text{ layers.}$$

In the present work, the catalysts were sulfided by a procedure using moderate conditions (H_2S = 10% vol, T = 623 K). Changing these conditions would probably provoke more drastic modifications in the catalyst morphology. Geometrical considerations relative to the MoS_2 crystallography and the shape of the MoS_2 platelets when they are formed on the support together with the changes in catalytic performance (for selected reactions such as thiophene hydrodesulfurization or propene hydrogenation) when the MoS_2 loading on the same γ-Al_2O_3 is increasing, have permitted the establishment of a model (47) that predicts the evolution of the relative number of active sites, assumed to be located at the edges of the slabs. In this model, it was proposed that the Mo loading increase should preferably lead to an increase in the elemental crystallite size instead of an increase in the total number of crystallites with the same size. The effect of stacking, which may reflect weaker interactions with the support surface, was not considered. It appears therefore interesting to draw the evolution of $\overline{N}$ as a function of $\overline{L}$ to detect any trend. Obviously if all the experimental data were plotted, they would cover a large part of the graph and it would not be so clear to see evidence for a relationship between $\overline{N}$ and $\overline{L}$. However, the lines drawn between selected data (Fig. 8) seem to indicate that $\overline{N}$ decreases when $\overline{L}$ increases. This correlation appears between samples 2 and 3 which differ only by the Mo loading; MoS_2 is less stacked but has higher length on the 2.4 Mo atom nm^{-2} sample (sample 3). Clearly the WS_2-γ-Al_2O_3 sample (no. 4) is quite different from the corresponding MoS_2-γ-Al_2O_3 sample (no. 3). This difference between MoS_2- and WS_2-supported catalysts is due not only to the changes in the nature of the oxometallates entities present in solution, $Mo_7O_{24}^{6-}$ and $W_{12}O_{40}^{6-}$, and adsorbed on the support during impregnation, but also to the effect of the sulfidation step which considerably modifies the chemical nature of the supported species. It was already noted (36) that supported polyoxotungstates are more difficult to sulfide than the corresponding polyoxomolybdates. The difference between Mo- and W-based catalysts is even more pronounced when the oxidic precursors have been dehydrated before sulfiding.

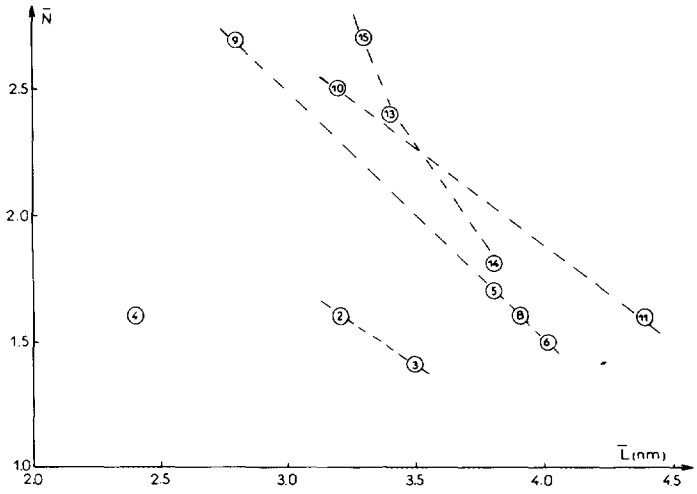

FIG. 8. Variation of the mean layer stacking $\overline{N}$ as a function of the mean length $\overline{L}$ of the disulfide crystallites observed for some of the studied catalysts.

The line going through samples 5, 6, 8, and 9 in Fig. 8 corresponds to the promoted samples with Co or Ni and on different supports (γ-Al_2O_3, $NiAl_2O_4$ or ZrO_2). It appears that introduction of Co or Ni induces similar morphological modifications of the supported MoS_2 crystallites. The changes of $\overline{L}$ and $\overline{N}$ could be considered as the result of the sulfidation of clumps of a given oxide which are generally described as supported isopolymetallate salt of Co or Ni (36). These features are also observed for the 2.5 Mo/NiAl sample, suggesting that initially incorporated Ni in the carrier is also available at least partly to promote the MoS_2 phase in agreement with previous results (38).

This effect is even more pronounced with zirconia. However, the variation of morphology implies a variation of the density of the supported crystallites. The tendency towards multilayer crystallites of ZrO_2 probably reflects the lower concentration of surface hydroxyl groups on zirconia compared to alumina. It appears that the density of surface hydroxyl groups is a parameter which can influence the MoS_2 layer stacking. This density may be managed by an appropriate choice of the carrier but also by modifying the surface state by introducing doping elements. Line 15–13–14 illustrates the influence of additives such as Cs, Na, or F on the MoS_2 phase deposited on the same support. Stacking is clearly influenced by the presence of F. Line 10–11 also gives evidence that the way P is introduced in the catalyst formulation has a decisive influence on the final sulfide phase morphology. Sample 4 (as already mentioned) and sample 7, where the support is $MgAl_2O_4$, or sample 12 are not connected with other samples. The data for samples 7 and 12 are therefore

not reported in Fig. 8. Nevertheless, it seems reasonable to assume that, within a given series, $\bar{N}$ decreases while $\bar{L}$ increases. Such an effect should be a consequence of the interactions between the MoS_2 platelets and the supports. At present, it is difficult to assign to a specific parameter of the support, e.g., nature of the exposed planes, number and strength of the hydroxyl groups, coordination of the uppermost cations, the key role for developing stacked MoS_2 crystallites with short length or, conversely, well-dispersed platelets with length higher than 4.0 nm. Another aspect to consider is the stabilization energy of nanocrystallites. This energy may be influenced by the orientation of the crystallites (basal plane) with respect to the exposed planes of the supports.

(iv) *Morphology Changes and Catalytic Activity Measurements*

A general question about supported active phases (metals, alloys, MoS_2 . . .) deals with the correlation which could exist between dispersion (i.e., morphology changes) and catalytic behaviour. The results presented here showed a similar evolution between tests I and II. The main effect appears when the promoting species (Co or Ni) are incorporated in the catalytic formulation. The promoters may modify the MoS_2 morphology (see the data for samples 5 or 6 in comparison with those for sample 3) but may also directly interact with the active sites at the edges of the platelets forming the well-known promoted Co–Mo–S or Ni–Mo–S phases (4, 6). Hence, morphological effects alone cannot account for the promoting effect observed for hydrogenation (HYD) of toluene. In this case, the electronic influence of the promoter is the main factor for explaining activity enhancements. By reference to sample 3, which contains only MoS_2 on the γ-Al_2O_3 support, samples 13, 14, or 15 have higher or lower activity depending on the nature of the additive. Sample 15 with F appears more active in both cases and sample 13 with Cs less active. On the line going through samples 13, 14, and 15 in Fig. 8, sample 13 is between samples 14 and 15. The changes of morphology in this series are not illustrated by changes in activity probably because the additives may also have a direct influence on the active sites (40); such an influence has already been noted when P is present in the catalyst formulation. Although it is not a metal promoter, the presence of phosphorus greatly increases the HDN ability as well the HYD of toluene (39). The results reported in Table 3 show that the HYD activity is improved upon introduction of P. This effect is more evident with the PMo catalyst. The structure of the adsorbed oxomolybdate entity is probably different as phosphomolybdate ions (i.e., $P_2Mo_5O_{23}^{6-}$, for example) (46) present in the impregnation solution may adsorb. Thus the stacking should be related to a more

TABLE 3

Activity Results in Toluene Hydrogenation

Catalyst number	Hydrogenation activity—Test I[a]	Hydrogenation activity—Test II[b]
1. Mo(4)/Al		
2. Mo(8)/Al		7×10^{-8}
3. Mo(14)/Al	1.04×10^{-7}	
4. W(21)/Al		
4'. 4 dehydrated prior to sulfidation		
5. CoMo/Al	6.6×10^{-7}	4.0×10^{-8}
6. NiMo/Al	1.25×10^{-6}	
6'. 6 dehydrated prior to sulfidation		
7. Mo/MgAl		
8. Mo/NiAl		
9. NiMo/Zr		1.65×10^{-7}
10. PMo/Al		2.5×10^{-7}
11. Mo/PAl		
12. NiMoP/Al	1.38×10^{-6}	5.0×10^{-8}
13. CsMo/Al	2.4×10^{-8}	6.5×10^{-8}
14. NaMo/Al	0.96×10^{-7}	7.5×10^{-8}
15. FMo/Al	1.46×10^{-7}[c]	

[a] Activity in (mol g^{-1} s^{-1}). In Test I 2% of thiophene is present in the feed.

[b] Activity in (mol g^{-1} s^{-1}). No sulfur-containing molecule is present in Test II.

[c] The result presented here corresponds to a catalyst similar to catalyst 15, which contains 1% F instead of 2% F.

complex distribution of the P, Mo, and S elements. The differences observed in the hydrogenation activity of toluene are therefore not yet understood. It appears that phosphorus participates in the architecture of the supported active phase and the difference in nature of the adsorbed phase should be invoked.

Recently, Daage *et al.* (48) have shown interesting data concerning the changes in selectivity during hydrodesulfurization of dibenzothiophene and the particle morphology of unsupported MoS_2 catalysts. In particular, they found a linear relationship between the ratio of the rate constants of hydrogenation into tetrahydrodibenzothiophene and the transformation into biphenyl, respectively, and the (002) diffraction linewidth, which is inversely correlated to the stacking of the MoS_2 layers. They discussed these results with a "rim-edge" model where hydrogenation reaction occurs exclusively on "rim" sites, whereas both "rim" and "edge" sites are involved in desulfurization. In the present paper such an analysis cannot be made because the extent of variation of stacked layers ($\bar{N}$) is too small (1.4 to 2.7 layers) compared with that observed on bulk sulfides and also because our model reaction is probably not sensitive enough to different locations of the active sites. Moreover, selectivity is not relevant for our test. It could be suggested that the use of large molecules able to develop a selectivity pattern during their transformation could be really beneficial for comparing the performances of supported MoS_2-based catalysts exhibiting different morphologies.

CONCLUSION

This systematic study by HREM of MoS_2- or WS_2-based catalysts has shown that different parameters such as the Mo loading, the presence of promoters or additives, and the nature of the support may have a real effect on the MoS_2 morphology. The mean length values $\overline{L}$ vary between 2.4 and 4.4 nm, whereas the mean layer stacking $\overline{N}$ varies between 1.4 and 2.7 layers. Within series of comparable samples, it appears that the decrease of stacking $\overline{N}$ induces a lateral growth of the supported platelets. This reflects modifications in the MoS_2-supported interactions and/or in the stabilization energy of the nanocrystallites of the Mo disulfide. No evident correlation has been obtained with the hydrogenation activity. The use of heavier molecules which can be selectively transformed could be beneficial for comparing this class of catalysts.

REFERENCES

1. Lepage, J. F., Cosyns, J., Courty, P., Freund, E., Franck, J. P., Jacquin, Y., Juguin, B., Marcilly, C., Martino, G., Miquel, J., Montarnal, R., Sugier, A, and van Landeghem, H., *in* "Catalyse de Contact," p. 441. Editions Technip, Paris, 1978.
2. Saito, M., and Anderson, R. B., *J. Catal.* **63,** 436 (1980).
3. U.S. Patents 4320030, 4491639 (Gas Research Institute); Denmark Patent 539679 (Haldor Topsøe); France Patent 8420069 (Gaz de France).
4. Massoth, F., *Adv. Catal.* **25,** 265 (1978).
5. Grange, P., *Catal. Rev.—Sci. Eng.* **21,** 135 (1980).
6. Hall, W. K., *in* "Proceedings, Third International Conference on the Chemistry and Uses of Molybdenum" (H. F. Barry and P. C. H. Mitchell, Eds.), p. 224. Climax Molybdenum Company, Ann Arbor, Michigan, 1982.
7. Topsøe, H., *in* "Surface Properties and Catalysis by Non-Metals" (J. P. Bonnelle and B. Delmon, Eds.), p. 329. Reidel, Dordrecht, 1983.
8. Delmon, B., *in* "Catalysis in Petroleum Refining" (D. L. Trimm *et al.*, Eds), p. 1. Elsevier, Amsterdam, 1990.
9. Topsøe, H., Clausen, B. S., Topsøe, N. Y., and Zeuthen, P., *in* "Catalysis in Petroleum Refining" (D. L. Trimm *et al.*, Eds.), p. 77. Elsevier, Amsterdam, 1990.
10. Schrader, G. L., and Cheng, C. P., *J. Catal.* **80,** 369 (1983).
11. Arnoldy, P., van den Heijkant, J. A. M., de Bock, G. D., and Moulijn, J. A., *J. Catal.* **92,** 35 (1985).
12. Payen, E., Kasztelan, S., and Grimblot, J., *J. Mol. Struct.* **174,** 71 (1988).
13. Payen, E., Kasztelan, S., Houssenbay, S., Szymanski, R., Grimblot, J., *J. Phys. Chem.* **93,** 6501 (1989).
14. Sanders, J. V., *in* "Catalysis, Science and Technology" (J. R. Anderson and M. Boudart, Eds), Vol. 7, p. 51. Springer-Verlag, Berlin, 1985.
15. Delannay, F., *Appl. Catal.* **16,** 135 (1985) and references therein.
16. Sanders, J. V., *Chem. Scr.* **14,** 141 (1978–79).
17. Sanders, J. V., and Pratt, K. C., *Micron* **11,** 303 (1980).
18. Sanders, J. V., and Pratt, K. C., *J. Catal.* **67,** 331 (1981).
19. Pollack, S. S., Sanders, J. V., and Tisher, R. E., *Appl. Catal.* **8,** 383 (1983).
20. Zaikovskii, V. I., Plyasova, L. M., Burmistrov, V. A., Startsev, A. N., and Yermakov, Y. I., *Appl. Catal.* **11,** 15 (1984).
21. Hayden, T. F., and Dumesic, J. A., *J. Catal.* **103,** 366 (1987).
22. Kemp, R. A., Ryan, R. C., and Smegal, J. A., *in* "Proceedings, 9th International Congress on Catalysis, Calgary, 1988" (M. J. Phillips and M. Ternan, Eds.), p. 128. Chem. Institute of Canada, Ottawa, 1988.
23. Mauchausse, C., Mozzanega, H., Turlier, P., and Dalmon, J. A., *in* "Proceedings, 9th International Congress on Catalysis, Calgary, 1988" (M. J. Phillips and M. Ternan, Eds.), p. 775. Chem. Institute of Canada, Ottawa, 1988.
24. Pratt, K. C., Sanders, J. V., and Christov, V., *J. Catal.* **124,** 416 (1990).
25. Hamon, D., Vrinat, M., Breysse, M., Durand, B., Beauchesne, F., and Des Courières, T., *Bull. Soc. Chim. Belg.* **100,** 933 (1991).
26. Ramirez, J., Castano, V. M., Leclercq, C., and Lopez-Agudo, A., *Appl. Catal.* **83,** 251 (1992).
27. Srinivasan, S., Datye, A. K., and Peden, C. H. F., *J. Catal.* **137,** 513 (1992).
28. Cruz-Reyes, J., Avalos-Borja, M., Farias, M. H., and Fuentes, S., *J. Catal.* **137,** 232 (1992).
29. Klier, K., *Catal. Today.* **15,** 361 (1992).
30. Dufresne, P., Payen, E., Grimblot, J., and Bonnelle, J. P., *J. Phys. Chem.* **85,** 2344 (1981).
31. Grimblot, J., Dufresne, P., Gengembre, L., and Bonnelle, J. P., *Bull. Soc. Chim. Belg.* **90,** 1261 (1981).
32. Kastelan, S., Grimblot, J., and Bonnelle, J. P., *J. Chim. Phys.* **80,** 793 (1983); *J. Phys. Chem.* **91,** 1503 (1987).
33. Payen, E., Kasztelan, S., Grimblot, J., and Bonnelle, J. P., *J. Raman Spectrosc.* **17,** 233 (1986).
34. Payen, E., Kasztelan, S., Grimblot, J., and Bonnelle, J. P., *J. Mol. Struct.* **143,** 256 (1986).
35. Payen, E., Kasztelan, S., and Grimblot, J., *J. Mol. Struct.* **174,** 71 (1988).
36. Ouafi, D., Mauge, F., Lavalley, J. C., Kasztelan, S., Houari, M., Grimblot, J., and Bonnelle, J. P., *Catal. Today.* **4,** 23 (1988).
37. Breysse, M., Cattenot, M., Decamp, T., Fréty, R., Gacher, C., Lacroix, M., Leclercq, C., de Mourgues, L., Portefaix, J. L., Vrinat, M., Houari, M., Grimblot, J., Kasztelan, S., and Bonnelle, J. P., *Catal. Today.* **4,** 39 (1988).
38. Payen, E., Kasztelan, S., Grimblot, J., and Bonnelle, J. P., *Catal. Today.* **4,** 57 (1988).
39. Poulet, O., Hubaut, R., Kasztelan, S., and Grimblot, J., *Bull. Soc. Chim. Belg.* **100,** 857 (1991).
40. Poulet, O., Doctoral thesis. Lille University, 1991.
41. Houssenbay, S., Payen, E., Kasztelan, S., and Grimblot, J., *Catal. Today.* **10,** 541 (1991).
42. Payen, E., Gengembre, L., Mauge, F., Duchet, J. C., and Lavalley, J. C., *Catal. Today.* **10,** 521 (1991).
43. Maugé, F., Duchet, J. C., Lavalley, J. C., Houssenbay, S., Payen, E., Grimblot, J., and Kasztelan, S., *Catal. Today* **10,** 561 (1991).
44. Breysse, M., Portefaix, J. L., and Vrinat, M., *Catal. Today.* **10,** 489 (1991).
45. Luck, F., *Bull. Soc. Chim. Belg.* **100,** 781 (1991).
46. Payen, E., Blanchard, P., Poulet, O., Grimblot, J., Hubaut, R., to appear.
47. Kasztelan, S., Toulhoat, H., Grimblot, J., and Bonnelle, J. P., *Appl. Catal.* **13,** 127 (1984).
48. Daage, M., Chianelli, R. R., and Ruppert, A. F., *in* "Proceedings, 10th International Congress on Catalysis, Budapest, 1992" (L. Guczi, F. Solymosi, and P. Tétényi, Eds.), p. 571. Akadémiai Kiadó, Budapest, 1993.